Running-in in fretting, transition from near-stable friction regime to gross sliding

Jouko Hintikka[a,b,1], Antti Mäntylä[a], Joona Vaara[a], Tero Frondelius[a,c], Janne Juoksukangas[b], Arto Lehtovaara[b]

[a] *R&D and Engineering, Wärtsilä, P.O.Box 244, 65101 Vaasa, Finland*
[b] *Tribology and Machine Elements, Faculty of Engineering and Natural Sciences, Tampere University, P.O. Box 589, 33101 Tampere, Finland*
[c] *University of Oulu, Erkki Koiso-Kanttilan katu 1, 90014 Oulu, Finland*

Abstract

It has been shown that quenched and tempered steel in gross-sliding fretting conditions, with tens of microns of slip amplitude, leads to fretting induced cracking and high and non-Coulomb friction. At low tangential load levels, there was only insignificant cracking. However, the running condition tends to change from stick to gross-sliding with a slip amplitude of a few micrometers. In this study, novel two-phase fretting experiments were done where quenched and tempered steel contact is run first at low loads that are initially in stick (running-in phase), followed by a gross-sliding phase with a slip amplitude of 35 μm. The results show that gross-sliding phase friction was reduced and the fretting induced cracks were shorter when the running-in phase was done at high enough load level and lasted more than 10^6 load cycles. At the highest running-in load levels, the resulting crack lengths were approximately halved in comparison to experiments without running-in, and it was possible to achieve nearly ideal Coulomb friction in the gross-sliding phase when the running-in duration was 10.2×10^6 load cycles. It is concluded that it is possible to control fretting-induced friction and cracking by carefully controlled running-in.

Keywords: Fretting, Running-in, Friction, Wear

1. Introduction

Waterhouse described fretting as the action of reciprocating surface sliding, causing types of damage known as fretting fatigue and fretting wear [1]. Often in fretting, the slip amplitude is only a few micrometers, though there is no specific upper limit for its magnitude. Typically, in fretting, the slip amplitude is small enough so that a significant proportion of the contact area remains in contact and unexposed to the atmosphere. This condition may be better described as reciprocating sliding if the slip amplitude is larger than the contact width. Fretting wear produces fine powdery wear debris, which tend to get entrapped in the interface. Fretting fatigue has been observed to be especially harmful type of damage. Fatigue failures in general can lead to catastrophic component failures though, in fretting, cracks nucleate easily and those can be difficult to detect without opening the contact. Furthermore, uncertainties related to fretting-induced friction and surface degradation make the evaluation of fretting fatigue loads difficult. [1–3].

Fretting contacts can be fully stuck, in partial-slip (PS) and in gross-sliding (GS), depending on the geometry, coefficient of friction (COF), used materials, and load [3, 4]. Stick or partial-slip may occur if the

[1] Corresponding author: jouko.hintikka@wartsila.com

friction force is less than the product of COF and normal force. A contact state where all points exhibit slippage is known as gross-sliding. It has been observed in experiments that the partial-slip condition, with high tangential load levels, tends to lead to fretting fatigue with a low fatigue life; however, in gross-sliding the fatigue life often increases. This increase in fatigue life in the gross-sliding regime has been explained by fretting wear wiping out crack embryos [5, 2]. However, simulations have shown that wear also increases the contact size which reduces stresses and moves the edge of the contact, which tends to be the most highly loaded location, effectively reducing damage accumulation [6].

Quenched and tempered steel can be used in components requiring high fatigue strength. In the case of large medium-speed combustion engines, among such components are the crank shaft and the connecting rod. Values and evolution of COF, in the case of quenched and tempered steel (EN 10083-1-34CrNiMo6+QT), have been reported numerous times utilizing sphere-on-plane and annular-flat-on-flat contact geometries [7–9]. Two types of non-ideal frictional behaviours have been identified and labeled non-Coulomb-friction and unstable-friction. Non-Coulomb friction is best observed in gross-sliding fretting loops where the tangential force increases substantially when the fretting motion approaches its extreme positions during individual fretting load cycles. This leads to 'hooked'-shaped fretting loops rather than parallelogram ones that ideal Coulomb friction would produce. Non-Coulomb friction has been explained to originate from tangential fretting scar interactions. Due to the non-ideal fretting loops shape, it has been suggested to use two COFs to give a better overall understanding of the fretting-induced friction. The COF that represents the maximum resistance against sliding during one load cycle is labeled as $COF_{\max}$, and average COF during a load cycle is labelled as COF_{mean}. Furthermore, both $COF_{\max}$ and COF_{mean} tend to change as a function of load cycles. A full description of the non-Coulomb friction can be found from Refs [10, 11].

The second non-ideality, unstable friction, has to do with the gradual reduction in the COFs as a function of load cycles [12]. Experiments with quenched and tempered steel have shown that $COF_{\max}$ peaks up to values of 1.5 during the first few hundreds of load cycles in gross-sliding conditions. After this, COFs exhibit gradual but significant reduction in their values (up to -50%). The threshold for the transition from a stable friction to the unstable friction was observed to occur when the average traction ratio, tangential traction divided by normal pressure (τ/p), was about 0.5 which is significantly lower than the measured maximum value of $COF_{\max}$ ($\approx$1.5). Very little and insignificant fretting damage was observed under stable friction conditions when the average traction ratio was below 0.5. However, the severity of fretting damage and magnitude of friction instability increased if the traction ratio was increased. Though the contact was initially in stick, the contact conditions changed gradually to gross-sliding. A simple explanation for this kind of behaviour is that the threshold corresponds to full stick conditions. It was suggested that this value could be taken as a design criterion for fretting-prone contacts. If more friction is required to guarantee stick conditions, the consequence may be unstable friction and fretting damage.

Wear experiments can typically be divided into three phases which are the running-in phase, steady-state-wear phase and wear-out phase [13, 14]. In the running-in phase, the wear rate tends to increase in a non-linear

fashion [13, 14], while the COF can reduce or increase [15–17]. In the steady-state-wear phase, the wear rate and COF tend to be stable and constant [13–17]. In the wear-out phase, the wear rate increases substantially. The wear rate during initial running-in and steady-state wear has been modeled using the exponential expression shown in Eq. 1 where the first part represents the exponential decay of wear rate during the running-in phase as a function of time (or sliding distance) and the K_3 represents the steady-state wear rate [13, 14].

$$wr(t) = K_1 e^{-K_2 t} + K_3 \tag{1}$$

According to Godet [18], motion between first bodies is accommodated via various mechanisms. Additionally, loose and solid 3rd body layers have a load carrying capacity, contributing to the wear between the first bodies and to friction [18]. Blau described that, for non-lubricated contacts, transitions in wear rate and in friction can occur due to processes such as metal transfer, film formation/removal, wear debris generation, and cyclic surface deterioration (surface fatigue) [19]. These transitions may occur suddenly or gradually. In fretting conditions, the slip amplitude tends to be low in comparison to the contact size, and large sections of the contact often remain closed, which enhances the role of wear debris entrapment on the friction and wear mechanisms [20]. It follows that the previously described non-Coulomb friction and unstable friction can be categorized as friction phenomena of the fretting contacts running-in phase.

An energy-based threshold has been empirically observed for the beginning of fretting wear for Hertzian contacts [21]. The threshold has been linked with the formation of a brittle tribologically transformed structure (TTS) layer, that has been reported for multiple metallic materials after fretting conditions [22, 23]. TTS nucleation has been reported to depend strongly upon the coefficient of friction and relative displacement [22]. General degradation layer (GDL) and TTS observations have been obtained typically using concentrated, Hertzian type, contacts producing high nominal load. In the case of flat-on-flat contact, the loads were nominally low; however, the fretting process itself leads to the formation of individual highly loaded 'spots', concentrating loads, where both TTS, GDL and cracking were present [24, 25].

In this study, it is investigated experimentally whether running-in can be used as a method to control fretting-induced friction and surface degradation, especially cracking. This study is largely a continuation of previously published work related to stable and unstable friction [12] where it was demonstrated that a quenched and tempered steel fretting contact can exhibit gross-sliding without producing the friction peak if the load level is low enough, albeit with very low slip amplitude of one or a few micrometers depending on the load level. A series of novel two-phase fretting-experiments were done where the contact was initially fretted at a low load level in comparison to loads measured at the beginning of gross-sliding conditions (labeled here as a running-in phase) followed by a gross-sliding fretting phase with a slip amplitude of 35 μm, without opening the contact in between the two phases. An analysis of frictional behaviour and fretting scar microscopy is presented.

2. Analytical

The fretting contact used in the experiments is of an annular flat-on-flat type, as illustrated in Figs.1 and 2,

the details of which are described in the Experimental section. Two identical specimens (Fig.2) are pressed against one another, and the fretting loading is a reciprocating rotation around the rotational symmetry axis of the specimen, producing tangential traction and slippage in the tangential direction. Here the necessary theory related to the mechanics of annular flat-on-flat contacts and relevant to this study is reproduced from [12].

2.1. Traction distributions

The normal and tangential traction distributions were studied by using the finite element method. The normal pressure was found to be about +18 % of the average value p_0 in the inner edge and -18 % in the outer edge of the specimen, and values varied nearly linearly as a function of radius r as shown in Eq. 2 where $K_s = -0.18$ (slope), $r_a = 10mm$, and $t = 5mm$ (thickness). The contact between tubes produces even contact pressure; however, the thicker part of the specimen with the conical seat (including the specimen holders) limits radial deformation, producing this deviation from constant normal pressure.

$$p(r) = p_0\,(1 + 2K_s(r - r_a)/t) \tag{2}$$

The annular contact used in the experiments can be in stick, partial-slip or gross-sliding, depending on the COF, normal force P, and torque amplitude T_a (or rotation amplitude θ_a). In stick, the tangential traction τ_{stick} is identical to the torque in a tubular cross-section, being defined by torque, radius, and torsional constant J_t that is equal to the polar moment of inertia in a circular cross-section (Eq.4). In gross-sliding, it (τ_{GS}) is equal to the product of normal pressure and COF (Eq.5).

$$J_t = I_p = \pi/2(r_o^4 - r_i^4) \tag{3}$$

$$\tau_{\mathrm{Stick}}(r) = rT/J_t \tag{4}$$

$$\tau_{\mathrm{GS}}(r) = \mathrm{COF}p(r) \tag{5}$$

Eq.4 shows that tangential traction increases linearly towards the outer edge of the specimen. However, tangential traction cannot exceed Eq.5. Therefore there will be partial slip once $\tau(r)/p(r) = COF$. The existence of partial slip is amplified further by the shape of the normal traction distribution having the lowest values at the outer edge of the specimen. A generic equation for tangential traction can be given as Eq.6.

$$\tau(r) = \min(\tau_{\mathrm{Stick}}(r), \tau_{\mathrm{GS}}(r)) \tag{6}$$

2.2. COF and traction ratio TR

The $COF_{\max}$ can be calculated from the measured fretting loops extracting the torque amplitude T_a as shown in Eq.8. In non-Coulomb conditions, COF_{mean} may give more realistic values, and it can be calculated using Eq.9 by extracting the frictional energy dissipation E_d and rotation amplitudes (θ_a) from fretting loops.

$$T_0 = 2\pi \int_{r_i}^{r_o} r^2 p(r)\, dr \tag{7}$$

$$COF_{\max} = T_a/T_0 \tag{8}$$

$$COF_{\mathrm{mean}} = E_d/[4\theta_a T_0] \tag{9}$$

These solutions hold true in gross-sliding in all points in the contact so that $\tau_{\max}(r)/p(r) = COF_{\max}$. However, in stick or in partial-slip, this is not true because the equation is valid only for sliding. Here we define the parameter traction-ratio (TR) that is used instead (Eq.10),

which stands for average τ/p-ratio in the contact. Contact surface area is A.

$$TR = (\tau/p)_{\text{mean}} = (2\pi/A)\int_{r_i}^{r_o} r(\tau/p)\,dr \qquad (10)$$

According to Ref [12] the TR produces values within 1 % of $COF_{\max}$ in all running-conditions. Therefore, $COF_{\max}$ is used in the analysis code instead. However, the term traction ratio TR is used to separate stick and partial slip-results from gross-sliding. In gross-sliding, $TR = COF_{\max}$, and in stick/partial-slip values of TR are nearly equal to $COF_{\max}$. However, TR is not a friction coefficient. In fact, $\tau(r)/p(r)$ values may deviate from $COF_{\max}$ values by up to ±40% though the average values are nearly identical. In experiments, TR and $COF_{\max}$ tend to reduce gradually as a function of load cycles (unstable friction). The maximum of TR during an experiment is labelled here as TRM, and it typically exists at the beginning of the experiment.

3. Experimental

3.1. Fretting apparatus

The experiments were done using an annular flat-on-flat fretting test device already described fully with illustrations in Refs [9, 11, 12]. Here only a brief description is given. The test device produced so-called plain fretting conditions, where all loads are carried by the fretting contact. Typically in fretting fatigue experiments, there exists bulk fatigue load which is absent in plain fretting conditions. The fretting contact occurs between two identical and axisymmetric specimens (Figs.1 & 2). One of the specimens is attached to a fixed specimen holder, and the other one to a detachable specimen holder. The detachable specimen holder is bolted

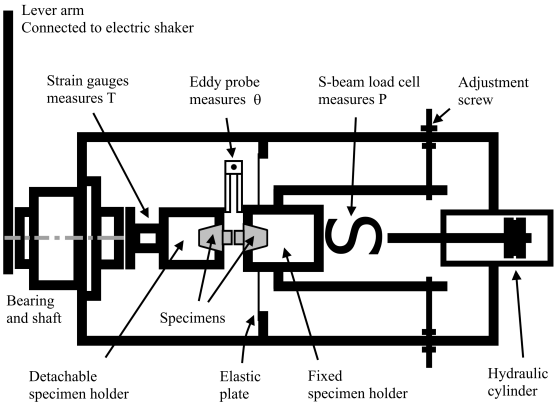

Figure 1: Annular flat-on-flat fretting apparatus

to a bearing unit that is rotated by an electric shaker. The detachable specimen holder also measures the torque T with strain gauges. The specimen parallelism is adjusted and measured with a pressure-sensitive film (Fuji Prescale) and by fine-tuning the fixed specimen holder orientation by tightening or loosening the adjustment screws. After the specimens are attached and aligned properly, the normal force is introduced with a hydraulic cylinder by deforming the elastic plate that attaches the fixed specimen holder to the apparatus frame until the desired normal pressure is achieved. The force required to deform the elastic plate was measured and removed in data post-processing, hence only the normal force P that affects the specimen is considered. The rotation θ_m between specimen holders is measured with an eddy current probe located at a distance of 100 mm from the rotation axis. The measured rotation includes specimen elastic deformation due to torque, which was removed numerically in post-processing using the expression in Eq.11 where k_s is the specimens' combined tangential stiffness.

$$\theta = \theta_m + k_s T \qquad (11)$$

Eq.11 represents the rotation between specimen surfaces from which an average slip amplitude is calculated using Eq.12 where r_a is specimen average radius of 10.0 mm.

$$u = \theta_m * r_a \tag{12}$$

Eqs.11 and 12 hold true for rigid bodies and are accurate for gross-sliding conditions with more than a few micrometers of slip amplitude also with elastic bodies. In partial slip conditions the average slip over the entire contact is also captured quite accurately [12]. Based on Eq.12, the rotation angle can be obtained by multiplying the presented slip amplitude values by a factor of 100 (1.0 μm $\rightarrow$ 0.1 mrad).

3.2. Specimens

The inner and outer radii (r_i and r_o) of the used annular contact were 7.5 mm and 12.5 mm respectively. The specimens were turned into shape from a 45 mm diameter steel rod (EN 10083-1-34CrNiMo6+QT). This material has a yield strength of 994 MPa and an ultimate strength of 1075 MPa. The contact surface was fine-ground so that the scratching marks were circular, hence parallel to the fretting movement. The specimens were cleaned thoroughly by using ultrasonic cleaner, first in acetone and then in ethanol. The arithmetic mean surface roughness S_a was in a range of [0.14-0.27] μm and the peak valley height S_t in a range of [1.8-4.9] μm.

3.3. Measurements

Measurements were run in two phases. The first was the running-in phase, followed by the gross sliding phase. In the running-in phase, the traction ratio was selected at levels in between stable friction and the peak of $COF_{\max}$, based on previous studies in gross-sliding

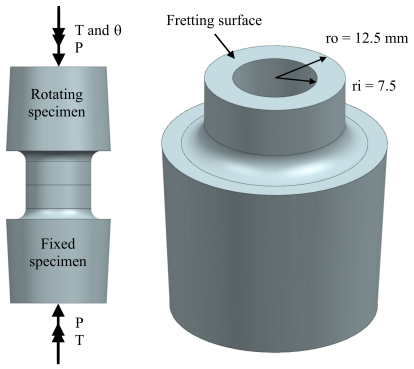

Figure 2: Specimen design

[11, 9] and in stick/partial-slip [12] and resulting in target TRM values of 0.56, 0.75 and 0.94. The duration of the running-in phase, N_1, was varied from 0.22×10^6 to 10.2×10^6 load cycles. The following gross-sliding phase had similar properties in all tests so that the target slip amplitude was 35.0 μm and its duration 3.02×10^6 load cycles for all tests. The normal pressure was 30 MPa in all tests. The test matrix is summarized in Table 1.

The experimental procedure mostly followed what is explained in detail in Ref [9] though some changes were done due to mid experiment loading change when the running-in transitioned to the gross-sliding phase. The running-in phase was set-up as follows. First, the specimens were attached to specimen holders, and the specimen parallelism was corrected by using pressure sensitive film. The target surface normal pressure was applied, and the rotation amplitude was increased linearly from zero to the target level during the first 10 s (400 load cycles), after which it was kept at a constant for the remainder of the running-in phase. The rotation amplitude levels were chosen so that the desired TRM was achieved. Once the running-in phase had accumulated the desired amount of load cycles, the apparatus was

Table 1: Measurement matrix

		Running-in		Gross sliding		
Test	P[N]	TRM[-]	$N_1[10^6]$	θ_a [mrad]	$u_a[\mu$m]	$N_2[10^6]$
1*	9318	0.56	10.2	3.89	38.9	3.02
2	9200	0.75	3.02	3.80	38.0	3.02
3*	9358	0.74	10.2	3.94	39.4	3.02
4	9466	0.93	0.22	3.91	39.1	3.02
5	9471	0.93	0.65	3.80	38.0	3.02
6	9369	0.94	3.02	3.93	39.3	3.02
7*	9330	0.94	10.2	3.89	38.9	3.02

shut down and new parameters were given for the control unit so that the desired 35.0 μm sliding amplitude was achieved. The values in Table 1 are higher because they represent the average values over the entire experiment. Measured rotation includes specimen elastic deformation which is dependent on the magnitude of friction, and therefore the actual slippage in the interface tends to increase when friction reduces because controlled rotation remains constant. Then the apparatus was restarted without dissembling the experiment, resulting in an additional 10 seconds long start-up phase. This procedure caused approximately a 20-minute mid-experiment halt due to resetting the control unit during which the contact remained closed and the normal load was maintained. In the experiments with 10.2×10^6 load cycles of the running-in phase, the procedure was updated so that the transition from the running-in phase to the gross-sliding phase was done on the fly with the same 10 seconds ramp-up to the target slip amplitude but without the mid-experiment shut-down. The experiments with updated procedure are marked with a star in Table 1. A description of the measurement data processing for Matlab is given in Refs [9, 11, 12]. The measurements were run in ambient laboratory atmosphere at 24 °C to 28 °C and at a relative humidity of 8 % to 24 %.

3.4. Pre- and post-experiment observations

The characterization of fretting scars and cross-sections followed the method presented in [24]. In short, after fretting tests, the specimens were washed in an ultrasonic device and then the contact surfaces were imaged with a stereomicroscope. The specimens were cleaned in an acid detergent to remove loose wear debris, and the surfaces were documented again with the stereomicroscope. Locations of severe fretting damage on the contact surfaces were chosen by visual observation, and two cross-section samples were made from one specimen of each test, resulting in the total of fourteen cross-section samples. The cross-section samples were etched after polishing to better reveal the microstructure and details. A Leica DM2500M and Zeiss ULTRAplus FESEM were used to study the cross-section samples. Intact surfaces and fretting scar surface profiles were measured by using a Wyco NT1100 3D-profilometer. The objectives used were a 5.0× main objective with a 0.5× field of view objective (effectively

2.5×) which gives an imaging area of 1.9 mm × 2.45 mm. Only the tilt was removed from the 3D surface profile before calculating the surface roughness, and no other filtering was used at all. Both single and stitched images ($1.9mm \times 4.6mm$) were taken in the surface profilometry.

4. Results and Discussion

4.1. TR and COF curves

Fig. 3 shows the evolution of TR during the running-in phase (A,C&E) and the subsequent $COF_{\max}$ in the gross-sliding phase (B,D&F) for all running-in load levels and durations. TRM stands for the maximum of TR during the experiment. In all the graphs, the black curves represent the experiments which were first run on a low TR level (running-in) followed by gross-sliding, and the line composition corresponds to the running-in duration. The graphs in the left (Fig. 3A, C&E) show the running-in phase TR as a function of the load cycles, and the previously determined TR levels required to achieve stable friction and the gross-sliding friction are shown as reference in grey (dash and dash-dot). The graphs in the right (Fig. 3B, D&F) show the subsequent gross-sliding $COF_{\max}$. The solid grey curve is the previously measured gross-sliding $COF_{\max}$ without the running-in phase, and the dashed grey line is a model fit described later. The grey box corresponds to the mid-experiment slip amplitude ramp-up (400 load cycles). Reference curves were reproduced from data already published in [9, 12].

At the lowest TR level, TR reduces from its initial value of 0.56 to about 0.50. This occurs simultaneously with a transition from stick to gross-sliding with a very low average slip amplitude of about 1.0 μm. After 10.2×10^6 load cycles of the running-in phase, the following gross-sliding phase $COF_{\max}$ behaviour is nearly identical to the reference curve without any running-in. The only notable differences between the two curves are that the experiment with the running-in shows slightly reduced peak value (1.40 vs 1.25) and that the peaking of the $COF_{\max}$ is slightly delayed (300 cycles vs 800 cycles). Once the $COF_{\max}$ had peaked, the friction curves are practically identical. The behaviour is quite similar with the second TR level of 0.75 though the peak friction is reduced and delayed even more. At the highest TR level of 0.93, the friction results are affected the most. During the running-in phase, the TR reduces from 0.93 to about 0.7. Again, this occurs simultaneously with a transition from stick to gross-sliding. At the end of the running-in phase, the average slip amplitude was about 3.0 μm. When the running-in duration was 0.22×10^6 load cycles, the resulting gross-sliding $COF_{\max}$ was quite similar to the experiment without any running-in. However, when the running-in duration was increased, the value of the friction peak was reduced. A running-in duration of 3.02×10^6 produced an insignificant friction peak, and no friction peak what so ever could be observed once the running-in duration was 10.2×10^6 load cycles. Again, the larger the reduction in $COF_{\max}$ the more load cycles were required for the peaking of friction to occur.

The peak $COF_{\max}$ values were collected from all test and are shown in Fig.4 as a function of running-in duration (A), running-in accumulated frictional dissipation (B), running-in accumulated slip (C) and number of gross-sliding load cycles needed to achieve the peak $COF_{\max}$ value (D). The reference data points represent the measurement without any running-in. All graphs show that the value of peak $COF_{\max}$ reduces exponen-

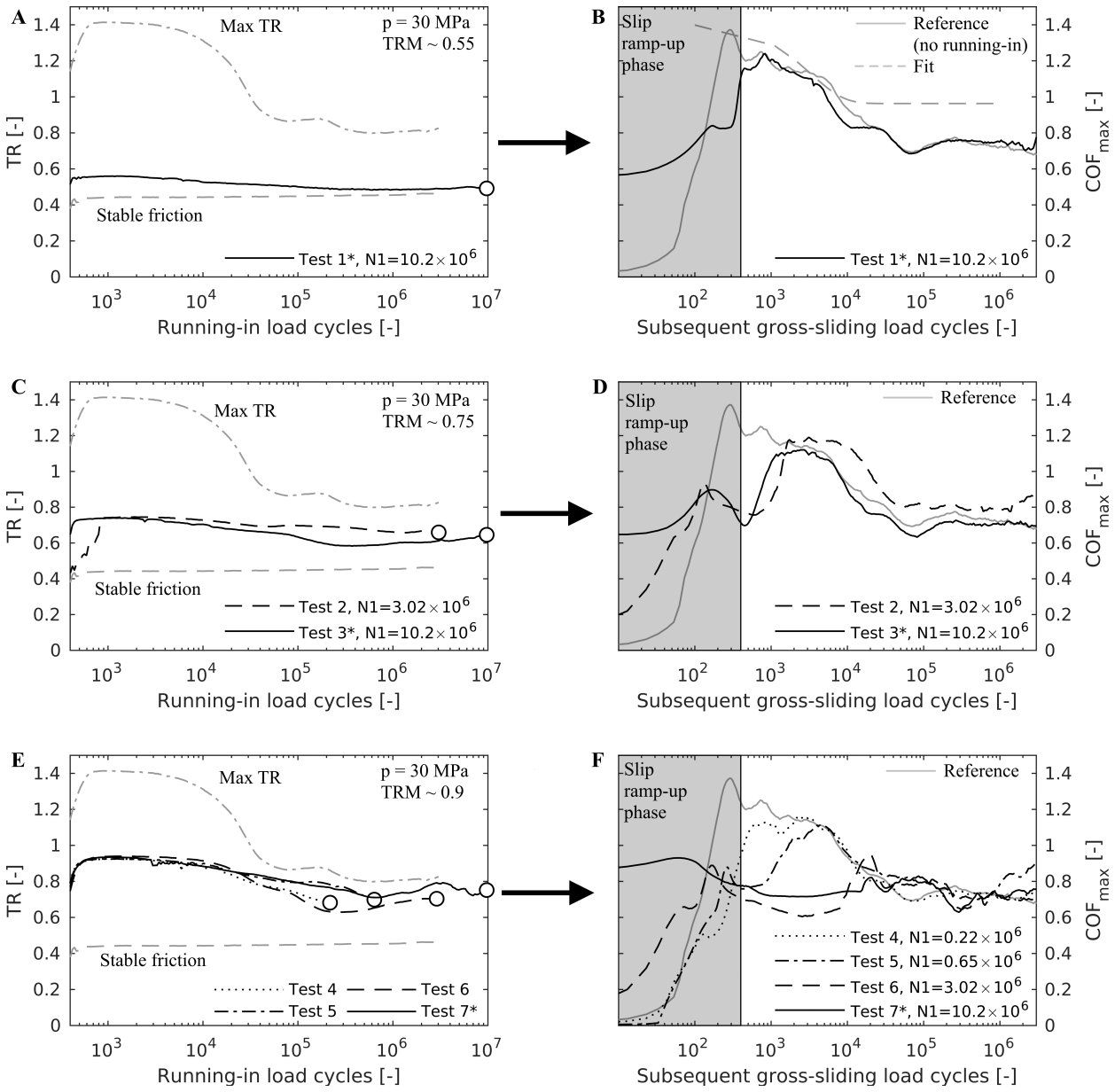

Figure 3: *TR* curves for initial running-in phase (left) and *COF* curves for subsequent gross-sliding phase (right). The contact was kept closed and under constant normal pressure in between the running-in and gross-sliding phases. A-B) Running-in and gross-sliding using TRM 0.55. C-D) Running-in and gross-sliding using TRM 0.55. E-F) Running-in and gross-sliding using TRM 0.9

.

tially and stabilizes to a steady state value. The shape of the $COF_{\max}$ decay is similar to the decay in the wear rate during the running-in in wear experiments, hence Eq. 1 can be used to describe its shape.

Fig. 4A shows how the peak $COF_{\max}$ reduces as a function of running-in load cycles. The reduction is largest with the highest TRM, the effect reducing with lowering running-in TMR. Also, most of the reduction

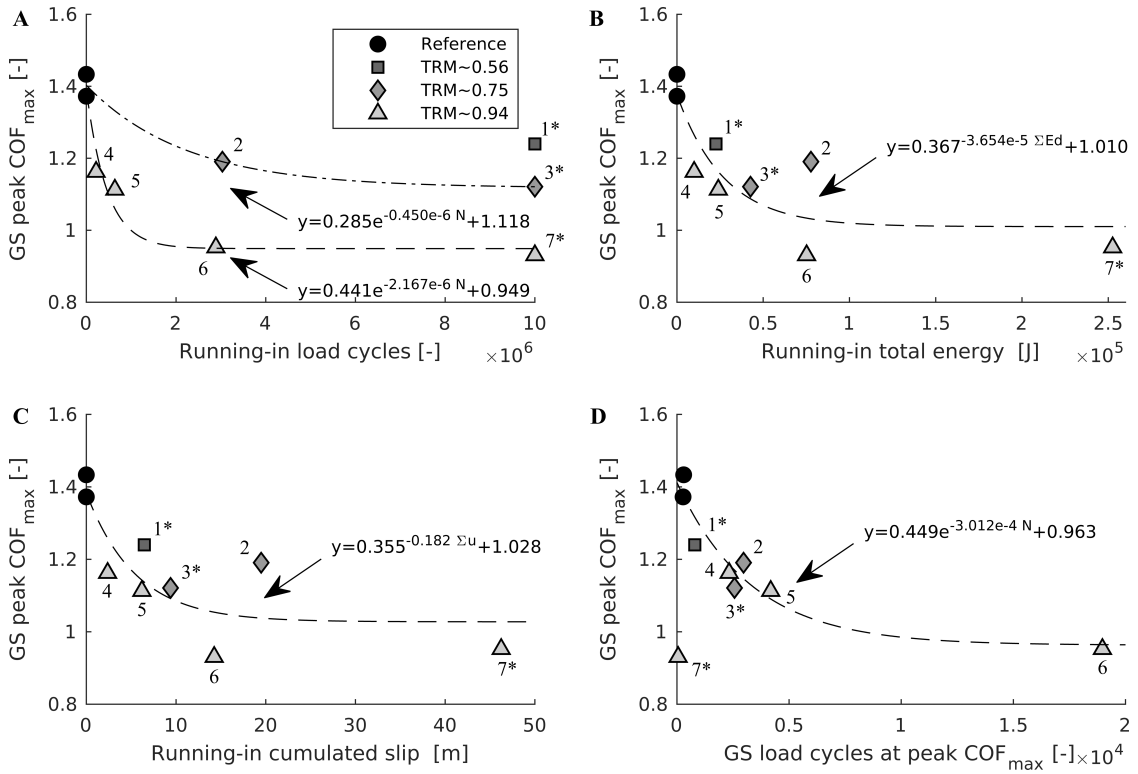

Figure 4: (A) Gross-sliding peak COF as a function of running-in duration and (B) Gross-sliding peak COF as a function of gross-sliding load cycles. Exponential decay function fitted to data based on Eq. 1, where time (t) was changed to number of load cycles (N). Number next to marker corresponds to test number in table-1

can be achieved with a running-in duration of about 10^6 load cycles. It remains uncertain whether it is possible to achieve a more substantial reduction in peak $COF_{\max}$ with low TRM levels if the running-in duration were increased. Fig. 4B&C shows the values of the gross-sliding phase peak friction as a function of running-in phase accumulated frictional energy dissipation ΣE_d and accumulated slip Σu. Both of these group the data quite nicely. It is possible that fretting wear or wear debris, or the fretting damage that accumulates during the running-in phase, leads to the observed reduction in the peak friction during the gross-sliding phase.

Fig. 4D shows the peak $COF_{\max}$ as a function of gross-sliding phase load cycles. It can be seen that the lower the peak $COF_{\max}$ was the more the friction peaking was delayed. The best fit of Eq. 1 to data is also included in Fig. 3B, showing that the peak $COF_{\max}$ follows closely the typical gross-sliding $COF_{\max}$ curve obtained without a running-in phase. It may be that there is an underlying mechanism that limits the $COF_{\max}$, which is a function of load cycles, such as accumulation of wear debris or accumulation of damage in the interface during the gross-sliding phase. The running-in phase already produces small amounts of wear debris and surface degradation in the asperity tip contacts. Any oxidized wear debris and surface layers may prevent contact between the first bodies, hence the the highest metal-to-metal adhesion-induced friction is avoided

during the early parts of the gross-sliding phase. Gradually, wear debris migrates due to fretting motion, and a delayed friction peak can occur. Highest friction peaking is achieved with virgin surfaces only.

The transition from the running-in to the gross-sliding phase was done using two methods. The first method had approximately a 20 minutes mid-experiment halt, whereas the second method had no halt at all. Hence it is possible that the change in the experimental procedure can have an effect on the results. One obvious effect is the cooling down of the specimens during the mid-experiment halt which is absent in the experiments without the halt. However, the frictional power was about 1 W at the highest running-in load level used, which causes an insignificant bulk temperature increase in the specimens; however, it is possible that the temperature is higher at the asperity tip scale. The friction results show that there is only little difference between gross-sliding COFs when the running-in duration was 3.02×10^6 (halt) and 10.2×10^6 (no halt). Also, a previous study in gross-sliding conditions with various slip amplitudes and normal pressure levels did not indicate any obvious temperature dependence although the frictional dissipation was an order of magnitude higher than 1 W [9].

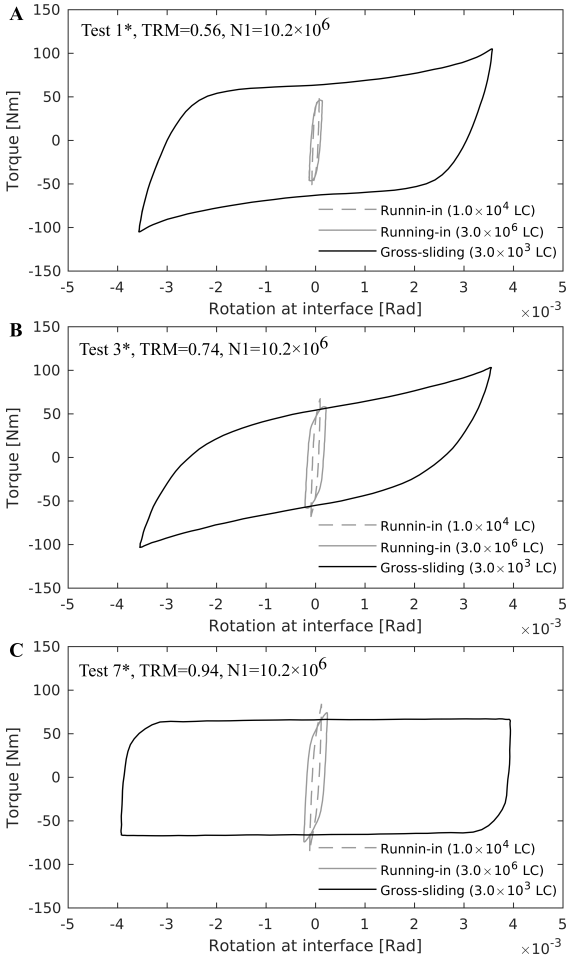

Figure 5: Measured fretting loops at different TRM levels where specimen elastic deformation was removed in post-test data analysis. All examples shown are from experiments where running-in duration was 10.2×10^6 load cycles.

4.2. Fretting loops

Examples of running-in and gross-sliding phase fretting loops are shown in Fig. 5 for all TRM levels used in this study. The grey lines represent the running-in phase and the black line the gross-sliding phase. The gross-sliding phase fretting loops shown were extracted exactly at 3000 load cycles, corresponding to the high friction phase.

It is seen from Figs. 5A-B that the gross-sliding phase produces highly non-Coulomb fretting loops. The fretting loops shape gradually transforms towards an ideal Coulomb one not-shown here, but examples can be found from [9]. However, Fig. 5C shows that the gross-sliding fretting loop is perfectly Coulomb when the running-in phase was run at the highest TRM level of 0.94 for 10.2×10^6 load cycles. Therefore it appears to be that the presence of a friction peak exists simultaneously with non-Coulomb friction.

4.3. Surface microscopy

All contact surfaces were imaged by using an optical microscope. Fig. 6 presents four fretting scar examples from different experiments.

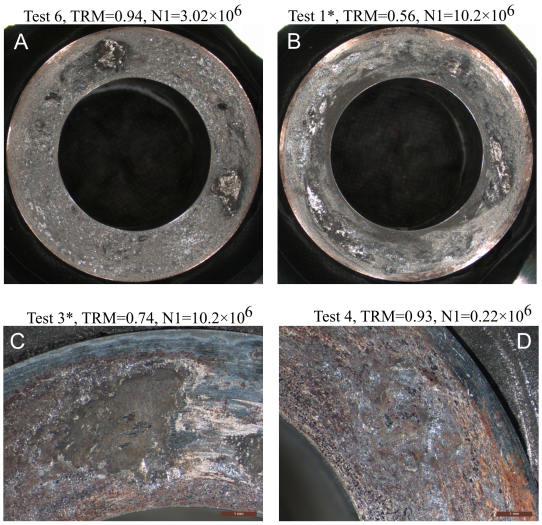

Figure 6: (A and B) Whole fretting scars of specimens of different TR and N1 before washing in acid detergent. (C and D). Higher magnification of suspected 'adhesion spots' observed after specimens were washed in acid detergent. Color image is available in the online version

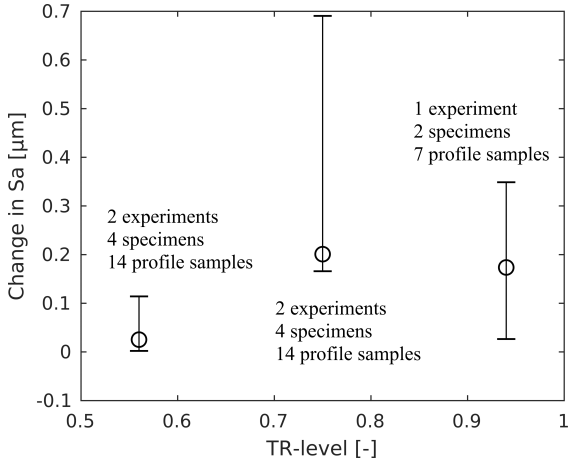

Figure 7: Surface roughness increase due to running-in based on [9]. Up to four surface roughness samples were taken from both specimens of each five tests which were available.

All fretting contact surfaces were thoroughly covered by fretting wear damage. At fist glance, surface damage was quite similar between these tests and the previous gross sliding tests without running-in [9]. In general, the scars have some reddish brown oxidation but are mostly grey and metallic in colour. All surfaces showed locations of adhesive wear, and a few millimetre sized marks of adhesion spots were identified in all specimens. Examples of places where cross-sections were made are shown magnified in Fig. 6C and D. Though the running-in phase had a significant effect on the COF, it was not possible to see any conclusive differences in the fretting scars due to the running-in. It is suspected that the 3.02×10^6 load cycles long gross-sliding phase causes so much fretting wear and surface degradation that all specimens look largely the same because each test had the same gross-sliding phase loading parameters.

Running-in-induced change in surface roughness was estimated from experiments already reported in Ref [12]. Though not reported at that time, post-test surface roughness was measured from the specimens which were available (a total of 5 experiments at TR levels of about 0.56, 0.75 and 0.93). Those test parameters correspond to the running-in phase load level used in this study. Up to four surface profiles were taken from each specimen, covering an area of $1.9 \times 4.6 mm^2$, so that the specimen surface was sampled almost from the inner edge to the outer edge while avoiding specimen edges. The change in the surface roughness due to fretting wear is shown in Fig. 7. It can be seen that surface roughness remains almost intact at the lowest TR level of 0.56 and increases when the TR level is increased; however, there exists quite a large scatter in the values. At the highest TR level of about 0.93, surface roughness has doubled from its original value. Though not

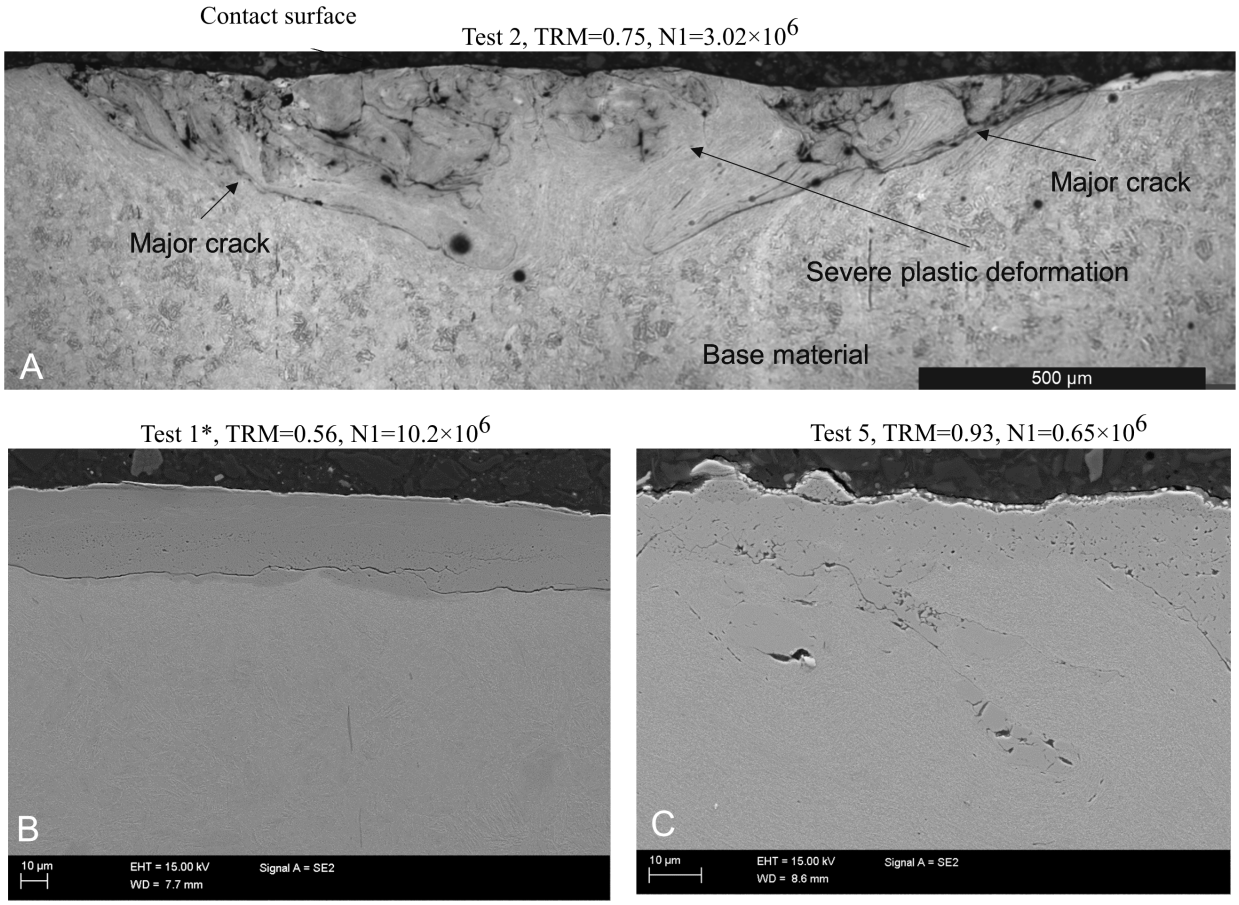

Figure 8: (A) Crack pair in the specimen with $TRM = 0.75$ and $N1 = 3.02 \times 10^6$, (B) degradation layers and cracking in specimens with $TRM = 0.56$ and $N1 = 10.2 \times 10^6$ and (C) $TRM = 0.93$ and $N1 = 0.65 \times 10^6$. Note that all images are from different samples.

shown here, surface profiles were taken from individual severely damaged fretting scar spots and Sa was often about 1.0 μm in such locations. Similarly, much of the contact remained intact and original grind marks were clearly visible (see Ref [12] for illustrations). Hence, an increase in surface roughness is caused by the combined effects of increased roughness in scarred locations and the increase in fretting scar coverage.

It is reasonable to assume that, during the running-in phase of this study, a similar type of increase in surface roughness and wear as a function of TR occurs as in the previous study [12]. In addition to the increase in the surface roughness, the increased wear at higher running-in load levels will lead to increased amounts of entrapped wear debris which can also have an effect on the gross-sliding phase friction and cracking.

4.4. Cross-sections microscopy

Cracking was found in every specimen, and the length of the largest crack in each specimen varied from about two hundred micrometers up to almost two millimetres. Smaller cracks were also encountered in all specimens. The biggest cracks formed a 'crack pair' similar to that found in previous tests [25]. Examples of the cracking and damage are shown in Fig. 8.

Plastic deformation occurs between the major cracks (Fig. 8A). Areas outside the major crack pair are largely intact base material. Fig. 8B and C show additional examples of surface degradation layers. Many samples had cracking in the degradation layers oriented in parallel with the surface (Fig. 8B) but not growing inwards the material like the cracks in Fig. 8A. These were close to the contact surface and may have contributed to the creation of wear debris. In addition, tribologically transformed structure (TTS) and third body layer (TBL) were present in many samples in the way already shown in [24].

4.5. Crack lengths

Crack lengths with different TRM values are presented in Fig. 9A. Only the longest cracks of each specimen are shown and cracks with a depth over 100 μm. The results indicate that the higher the TR ratio during the running-in phase the shorter are the resulting cracks though one result shows a contrary behaviour; however, this test point corresponds to the shortest running-in duration. At the lowest TRM value (0.55), clear crack pairs were found. The COF behaviour was similar compared to the gross sliding test with similar (gross sliding) parameters and without any running-in, and also the crack dimensions were at a similar level between these tests [25]. Thus, this suggests that the running-in phase should be done with sufficiently high loading in order to obtain reduction in the fretting-induced cracking.

There is a slight indication of a decrease in crack length as the maximum value of gross sliding $COF_{\max}$ decreases (Fig. 9B). This could be explained by a decreased local loading resulting from decreased adhesion during the gross-sliding phase. However, the crack dimensions seem not to correlate with the amount of running-in load cycles. Fig. 9C shows the crack length as a function of running-in phase accumulated energy, and here no clear correlation can be seen between the parameters. This may indicate that the running-in TMR level largely determines the reduction in the adhesion spot crack lengths. Though it may be that running-in duration also plays a role on the resulting crack lengths; however, such effects could not be observed conclusively from these experiments. A series of test with smaller amount of running-in load cycles could reveal such load cycle dependencies.

Adhesion spots typically have a crack pair, and the cracking occurs at the edges of the adhesion spot in a perpendicular direction to the fretting motion. There is a strong correlation between the crack pair width and the resulting crack lengths, as illustrated in Fig. 9D, so that the the larger the adhesion spot the longer the cracks are. Additionally, the slope of the linear regressions is identical to the one shown in Ref [25]. It may be that the surface modifications related to the running-in phase tend to limit the adhesion spot size that can develop during the gross-sliding phase; however, it does not prevent it. Therefore, a full understanding of fretting induced adhesion spot cracking requires more research on the very formation and properties of the adhesion spot. No crack pair was observed in test-3*. However, the crack found was located at the edge of the sample, hence it is possible that its crack pair existed but was not included in the cross-section sample.

5. Conclusions

Two-phase plain fretting experiments were done without opening the contact between the two phases.

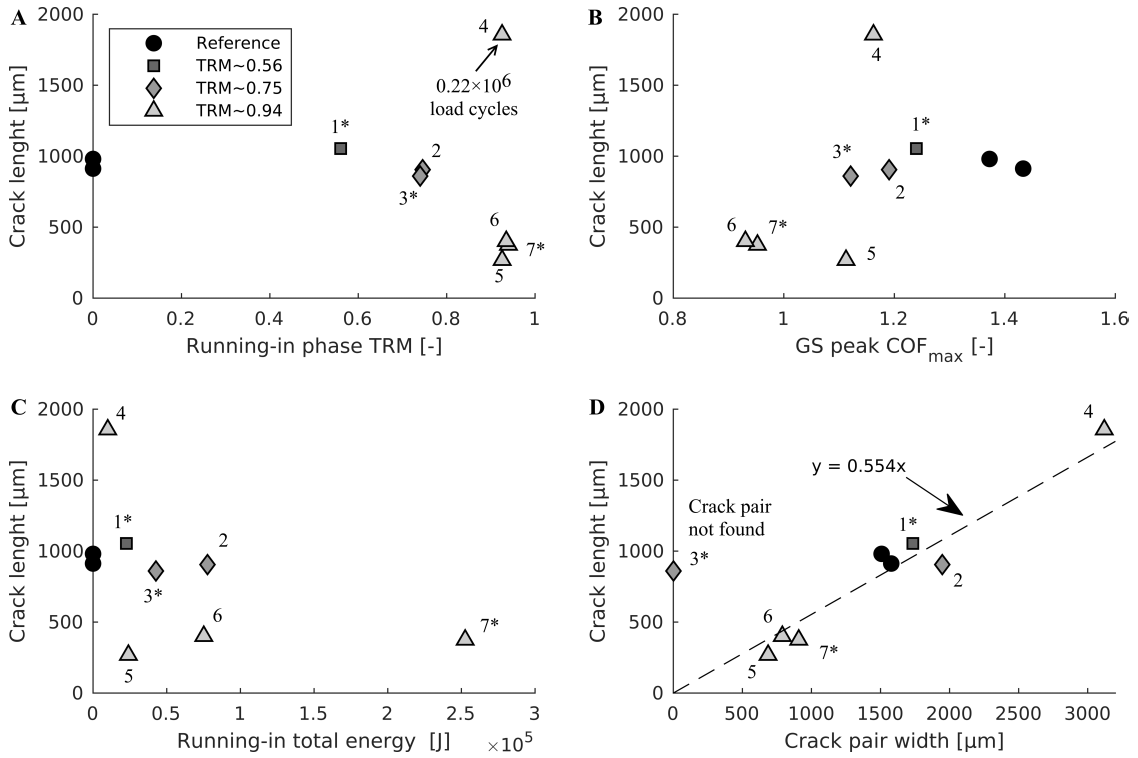

Figure 9: Largest cracks found as a function of (A) running-in phase TRM, (B) gross-sliding phase peak $COF_{\max}$, (C) running-in phase accumulated frictional energy, and (D) width of the crack pair. Number next to marker corresponds to test number.

In the first phase, the contact was run-in using a low enough load level to achieve stick conditions, though due to an unstable friction the contact transitioned gradually to gross-sliding with a low slip amplitude. The running-in phase load level and duration were varied. The second phase was in gross-sliding with a large slip amplitude of 35 μm and duration of 3.02×10^6 load cycles in all tests. Following conclusions were obtained:

- It is possible to control gross-sliding phase friction by selecting the running-in phase test parameters carefully. The gross-sliding phase produced stable and ideal friction when the running-in phase duration was long enough ($> 10^6$ load cycles) and the load level high enough (close to steady state gross-sliding friction). However, with a brief running-in phase duration or low load level resulted in non-Coulomb friction and high friction values in the gross-sliding phase which were quite similar to what has been measured with virgin surfaces. It is suspected that the extend of surface degradation and wear debris accumulation during the running-in phase plays a key role in this observed friction behaviour.

- At first glance, the fretting scar surfaces look alike in surface microscopy because in all tests they were subjected to 3.02×10^6 load cycles in gross-sliding conditions with an identical load regardless of the running-in phase. Fretting scar cross-sections revealed that there are cracks in the specimens and that the crack length was de-

pendent on the running-in phase test parameters. The higher the running-in phase TRM the shorter the crack lengths were. Observed crack lengths were strongly dependent on the adhesion spot sizes, hence in order to reduce the fretting induced cracking, it is important to limit the formation and growth of adhesion spots. This can be accomplished by carefully performing the running-in phase with similar mechanisms that have positive effects on friction as well.

6. Acknowledgements

This study was conducted as a part of the MaNuMiES (Dnro 3361/31/2015) and WIMMA (Dnro 1566/31/2015) research projects. The authors are grateful for the financial support provided by Business Finland Oy (former Tekes), Wärtsilä Finland Oy, Agco Power Oy and Global Boiler Works Oy.

References

[1] R. Waterhouse, Fretting corrosion, Pergamon press, Oxford, ISBN 0 08 16902 3, 1972.

[2] D. Hills, Mechanics of fretting fatigue, Kluwer Academic Publishers, ISBN 0-7923-2866-3, doi:https://doi.org/10.1016/0043-1648(94)90173-2, 1994.

[3] K. Johnson, Contact Mechanics, Cambridge University Press, Cambridge, ISBN 0 08 16902 3, 1985.

[4] L. Vincent, Y. Berthier, M. Dubourg, M. Godet, Mechanics and materials in fretting, Wear 153 (1) (1992) 135 – 148, ISSN 0043-1648, doi:https://doi.org/10.1016/0043-1648(92)90266-B.

[5] O. Vingsbo, S. Söderberg, On fretting maps, Wear 126 (2) (1988) 131–147.

[6] J. Madge, S. Leen, I. McColl, P. Shipway, Contact-evolution based prediction of fretting fatigue life: effect of slip amplitude, Wear 262 (9-10) (2007) 1159–1170.

[7] A. Pasanen, A. Lehtovaara, R. Rabb, P. Riihimäki, Friction behavior of quenched and tempered steel in partial and gross slip conditions in fretting point contact, Wear 267 (12) (2009) 2200–2207.

[8] J. Hintikka, A. Lehtovaara, C. Lönnqvist, Effect of start-up schemes and amplitude of tangential motion on friction behavior in fretting point contact, Tribology International 44 (11) (2011) 1535–1543.

[9] J. Hintikka, A. Lehtovaara, A. Mäntylä, Fretting-induced friction and wear in large flat-on-flat contact with quenched and tempered steel, Tribology International 92 (2015) 191 – 202, ISSN 0301-679X, doi: https://doi.org/10.1016/j.triboint.2015.06.008.

[10] D. Mulvihill, M. Kartal, A. Olver, D. Nowell, D. Hills, Investigation of non-Coulomb friction behaviour in reciprocating sliding, Wear 271 (5) (2011) 802 – 816, ISSN 0043-1648, doi: https://doi.org/10.1016/j.wear.2011.03.014.

[11] J. Hintikka, A. Lehtovaara, A. Mäntylä, Normal displacements in non-Coulomb friction conditions during fretting, Tribology International 94 (2016) 633 – 639, ISSN 0301-679X, doi: https://doi.org/10.1016/j.triboint.2015.10.029.

[12] J. Hintikka, A. Mäntylä, J. Vaara, T. Frondelius, A. Lehtovaara, Stable and unstable friction in fretting contacts, Tribology International 131 (2019) 73 – 82, ISSN 0301-679X, doi: https://doi.org/10.1016/j.triboint.2018.10.014.

[13] R. Kumar, B. Prakash, A. Sethuramiah, A systematic methodology to characterise the running-in and steady-state wear processes, Wear 252 (5-6) (2002) 445–453.

[14] K. Lijesh, M. Khonsari, On the onset of steady state during transient adhesive wear, Tribology International 130 (2019) 378–386.

[15] A. Akchurin, R. Bosman, P. M. Lugt, Generation of wear particles and running-in in mixed lubricated sliding contacts, Tribology international 110 (2017) 201–208.

[16] H. Cao, X. Zhou, X. Li, K. Lu, Friction mechanism in the running-in stage of copper: From plastic deformation to delamination and oxidation, Tribology International 115 (2017) 3–7.

[17] S. Hu, N. Brunetiere, W. Huang, X. Liu, Y. Wang, The bi-Gaussian theory to understand sliding wear and friction, Tribology International 114 (2017) 186–191.

[18] M. Godet, The third-body approach: a mechanical view of wear, Wear 100 (1-3) (1984) 437–452.

[19] P. J. Blau, Mechanisms for transitional friction and wear behavior of sliding metals, Wear 72 (1) (1981) 55–66.

[20] Y. Berthier, L. Vincent, M. Godet, Velocity accommodation in

fretting, Wear 125 (1-2) (1988) 25–38.

[21] S. Fouvry, T. Liskiewicz, P. Kapsa, S. Hannel, E. Sauger, An energy description of wear mechanisms and its applications to oscillating sliding contacts, Wear 255 (1-6) (2003) 287–298, doi: https://doi.org/10.1016/S0043-1648(03)00117-0.

[22] Z. Zhou, E. Sauger, J. Liu, L. Vincent, Nucleation and early growth of tribologically transformed structure (TTS) induced by fretting, Wear 212 (1) (1997) 50–58, doi: https://doi.org/10.1016/S0043-1648(97)00141-5.

[23] E. Sauger, L. Ponsonnet, J. Martin, L. Vincent, Study of the tribologically transformed structure created during fretting tests, Tribology International 33 (11) (2000) 743–750, doi: https://doi.org/10.1016/S0301-679X(00)00088-8.

[24] V. Nurmi, J. Hintikka, J. Juoksukangas, M. Honkanen, M. Vippola, A. Lehtovaara, A. Mäntylä, J. Vaara, T. Frondelius, The formation and characterization of fretting-induced degradation layers using quenched and tempered steel, Tribology International 131 (2019) 258–267.

[25] J. Juoksukangas, V. Nurmi, J. Hintikka, M. Vippola, A. Lehtovaara, A. Mäntylä, J. Vaara, T. Frondelius, Characterization of cracks formed in large flat-on-flat fretting contact, International Journal of Fatigue 124 (2019) 361–370.